

# Alternate surface measurements for GMT primary mirror segments

J. H. Burge<sup>a,b</sup>, L. B. Kot<sup>a</sup>, H. M. Martin<sup>a</sup>, C. Zhao<sup>b</sup>, T. Zobrist<sup>b</sup>

<sup>a</sup>Steward Observatory, University of Arizona, Tucson, AZ 85721, USA

<sup>b</sup>College of Optical Sciences, University of Arizona, Tucson, AZ 85721, USA

## ABSTRACT

The primary mirror for the 25-m Giant Magellan Telescope is made of seven circular segments, each of 8.4-m diameter. The lack of axisymmetry and the steep aspheric departure present significant technical challenges for the metrology. These segments will be measured interferometrically using a complex system of mirrors and holograms to give a null test with high spatial resolution. While analysis predicts this system will meet requirements, an additional set of measurements will be used to corroborate the principal interferometric measurement. The set of tests, including these alternate surface measurements, assures that all aspects of the mirror surface are measured completely and redundantly. The corroboration tests discussed in this paper are:

- Direct surface profile using metrology system based on a laser tracker, measuring low order shape errors
- Shear testing with full aperture interferometer, separating small scale errors in the null test from those in the mirror
- Slope testing with scanning pentaprism, measuring low order shape errors and sampling small scale errors

**Keywords:** telescopes, optical fabrication, optical testing, aspheres

## 1. INTRODUCTION

The 25-m primary mirror for the Giant Magellan Telescope GMT is made of seven 8.4-m segments.<sup>1</sup> An optical test is being developed for the off-axis segments that uses a large 3.8-m tilted mirror to fold the light path and to compensate the 14.5 mm of aspheric departure.<sup>2</sup> We recognize the importance of corroborating the measurements from the principal optical test to insure that the correct surface is manufactured.

We are developing a set of independent tests that provide such redundancy in a cost effective way for GMT. The first of these systems is a laser tracker based measuring system that acts as a coordinate measurement system. In addition to using this system to guide rough figuring, we expect to improve the quality of the data to provide accurate measurements of low order shape errors in the mirror segment. A second system for measuring global figure reflects a laser beam off the surface and captures the return to measure surface slope. A scanning pentaprism is used with this system to provide laser illumination with sufficient accuracy.

The principal optical test for these mirrors uses a set of mirrors and computer generated hologram (CGH) to provide a null corrector for full-aperture interferometry. We can measure high frequency errors in this test system directly by using a shear test. By making several measurements where the test optics are stationary and the GMT mirror segment is moved, small scale errors from the test can be decoupled from this in the mirror. The GMT segments are off-axis portions of an axisymmetric parent, allowing a natural motion for this test defined as the rotation about the parent axis.

The designs, analysis, and predicted performance of these alternate measurements are discussed in the following sections.

## 2. DIRECT SHAPE MEASUREMENT USING LASER TRACKER

The optical surface will be measured using a commercial laser tracker mounted above the mirror in the test tower. The laser tracker is a three-dimensional coordinate measurement system that tracks a retroreflector and uses the combination of gimbal angles and line of sight distance to determine the position of the retroreflector. Variations in the line of sight distance are accurately measured using the distance measuring interferometer (DMI) built into the laser tracker. To measure the surface we move a SMR (sphere-mounted retroreflector) across the surface and use the DMI to measure the relative change in distance. This system, shown in Figure 1, provides two important measurements:

- It does not require a specular surface, so we can use this system to measure the rough surface to guide the generating and loose abrasive grinding operations.
- We can measure low order shape errors in the polished surface to  $< 1 \mu\text{m}$  by augmenting the laser tracker with additional references, calibrating the tracker errors, and measuring multiple points across the mirror to reduce the effects of noise. This provides an independent corroboration of the mirror shape.

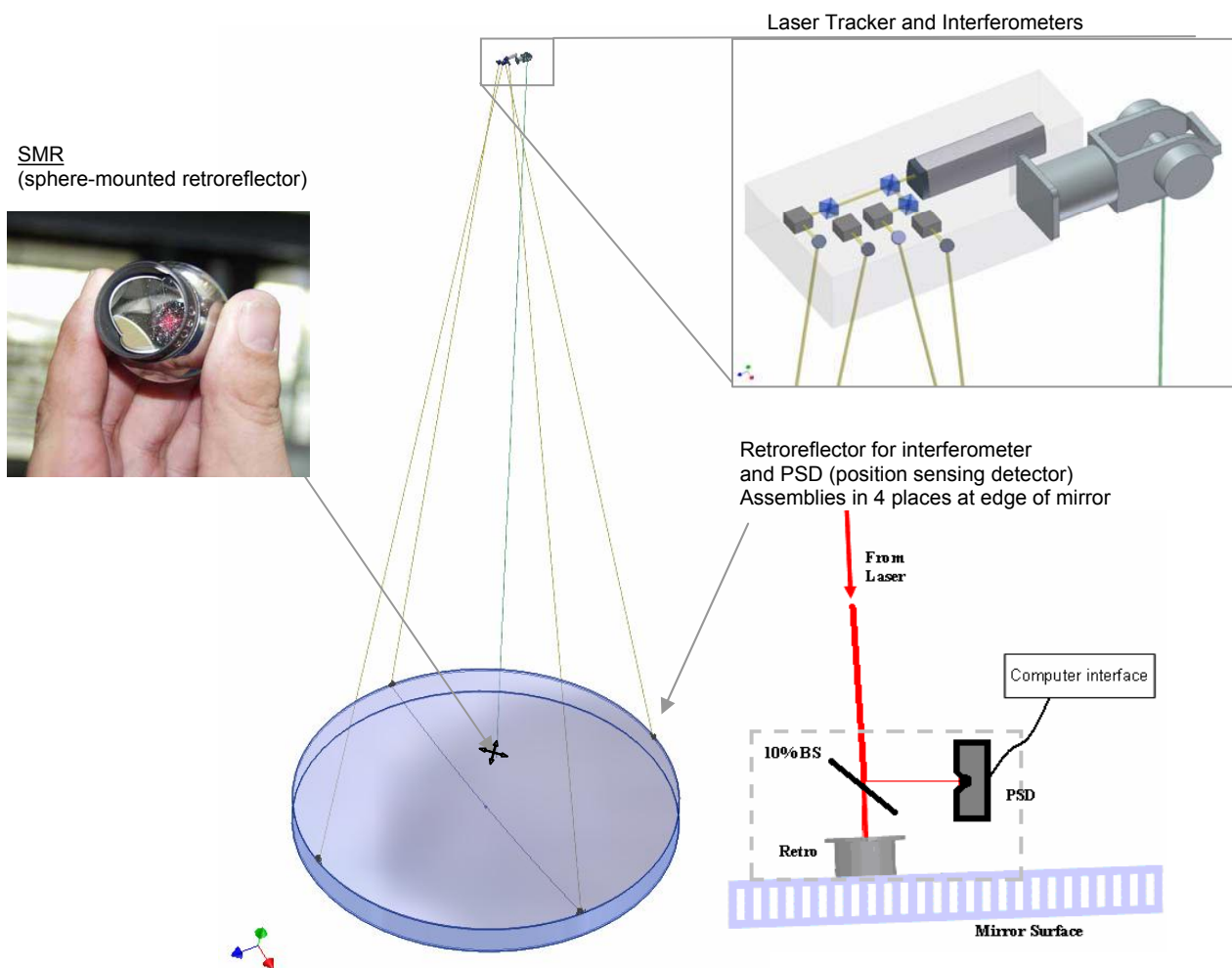


Figure 1. Conceptual drawing of the laser tracker set up for measuring the mirror surface. The laser tracker uses interferometry to measure distance to an SMR (sphere-mounted retroreflector). The tracker runs under servo control to follow the ball as it is scanned across the surface, combining radial distance with the gimbal angles to make a three-dimensional measurement. Effects due to the combined motion of the air, mirror, and tracker are mitigated by separate real-time measurements of distance and lateral motion using four interferometer/position sensing detector systems.

A laser tracker is a metrology tool which measures and maps a system of points in three dimensions. The tracker achieves this through the use of an internal Distance Measuring Interferometer (DMI) which monitors the return from a spherical mounted retroreflector (SMR). A two-axis gimbaled mirror coupled to an internal Position Sensing Detector (PSD) form a feedback loop which follows the SMR as it is moved. The internal DMI continually monitors the radial distance from the laser tracker head to the SMR, while a pair of encoders monitor the azimuth and elevation of the beam. These three measurements define the SMR's position in three-space with respect to the tracker.

The system for moving the SMR across the surface of the mirror has not yet been designed. Previous projects have used simple manual systems which become difficult for such a large mirror. We need to move the 1.5-inch SMR to ~300 discrete locations distributed uniformly across the 8.4-m mirror without damaging the mirror or disrupting the laser beams from the tracker or any of the four reference DMIs. We do not require accurate lateral positioning. We are investigating the use of an air bearing with simple cable-drive mechanism.

The laser tracker has excellent accuracy and resolution for the line of sight distance, as measured with the DMI, but the angular measurements are less precise. Ideally, the tracker would be mounted at the center of curvature of the optic, which minimizes the sensitivity to angles. In practice, this point is not easily accessible, so we locate the system as far away as possible. The geometry for this system is shown in Figure 3. The angle  $\alpha$ , which describes the deviation of the line of sight from the surface normal is calculated approximately for a spherical mirror, assuming small angles:

$$\alpha \cong \arcsin\left(\frac{x}{h}\right) - \arcsin\left(\frac{x}{R}\right) \cong x\left(\frac{1}{h} - \frac{1}{R}\right). \quad (\text{Eq. 1})$$

Using this, the sensitivity of the surface measurement to position on the mirror  $x$  is calculated as  $\frac{dr}{dx} = \alpha \cong \frac{x(R-h)}{hR}$  where  $dr$  represents the change in the line of sight distance as measured by the DMI.

The GMT test with the tracker 22 m above the mirror has sensitivity of 75  $\mu\text{m}/\text{mm}$  at the outer edge of the mirror, and an average sensitivity to radial position of 53  $\mu\text{m}/\text{mm}$ .

The sensitivity of the surface measurements to angular error in the line of sight of the tracker is calculated as

$$\frac{dr}{d\theta} \cong \alpha \cdot h \cong \frac{x}{R}(R-h) \quad (\text{Eq. 2}).$$

The GMT test has sensitivity to angle of 1.7  $\mu\text{m}/\mu\text{rad}$  or 0.6  $\mu\text{m}/\text{arcsec}$  at the outer edge of the mirror, and an average sensitivity to angle of 0.37  $\mu\text{m}/\text{arcsec}$ .

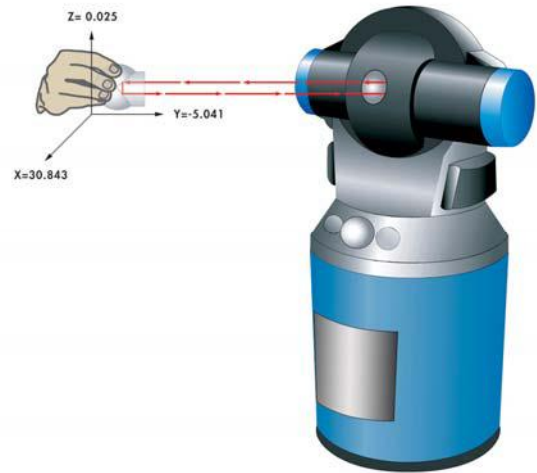


Figure 2. Laser tracker head with internal distance-measuring interferometer that measures the distance and angles to the SMR. Copyright © 2006 FARO Technologies Inc. All Rights Reserved.

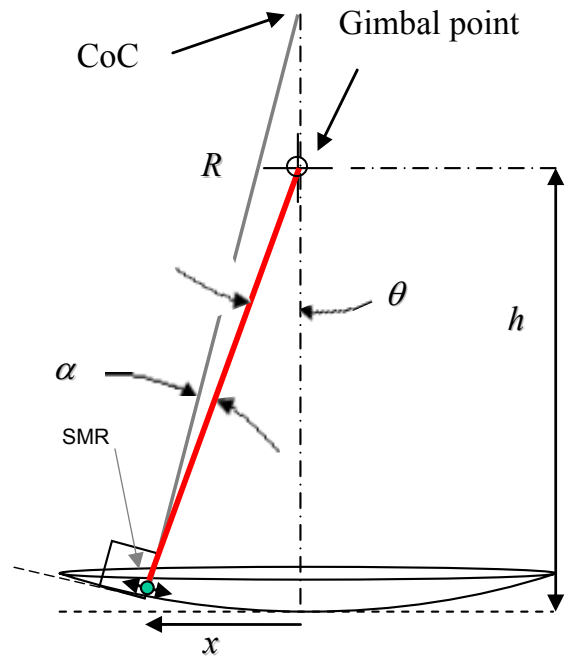


Figure 3. By placing the laser tracker near the center of curvature, the measurements are made at near-normal incidence and the sensitivity to errors in the angles is minimized.

The measurement errors due to the tracker can be reduced by a combination of calibration for systematic errors and averaging for noise. Systematic errors in the tracker can be calibrated to the noise limit using a set of measurements with a small spherical reference mirror. Treating the lowest order errors in the laser tracker,

$$\varepsilon(\theta_x, \theta_y) = \Delta r(\theta_x, \theta_y) + \frac{dr}{d\theta_x}(\theta_x, \theta_y) \cdot \Delta\theta_x(\theta_x, \theta_y) + \frac{dr}{d\theta_y}(\theta_x, \theta_y) \cdot \Delta\theta_y(\theta_x, \theta_y), \quad (\text{Eq. 3})$$

where,

$\varepsilon(\theta_x, \theta_y)$  is the tracker measurement error as a function of the two gimbal angles,

$\Delta r(\theta_x, \theta_y)$  is the systematic tracker error in the radial (interferometer) direction,

$\Delta\theta_x(\theta_x, \theta_y)$  is the systematic angular tracker error in the  $x$  direction,

$\frac{dr}{d\theta_x}(\theta_x, \theta_y)$  is the sensitivity to gimbal angle due to the non-normal line of sight, as calculated in Eq. 2.

The systematic errors in the tracker,  $\Delta r(\theta_x, \theta_y)$ ,  $\Delta\theta_x(\theta_x, \theta_y)$ , and  $\Delta\theta_y(\theta_x, \theta_y)$ , can be measured directly using a spherical reference surface. As these errors do not depend on the radius of the sphere, they can be calibrated by using the tracker to measure a small spherical surface near the tracker. With a set of three separate measurements, each spanning the  $(\theta_x, \theta_y)$  space, it is possible to determine the three functions describing first order errors in the tracker. The optimal three measurements are performed according to the steps below, and as shown in Figure 4.

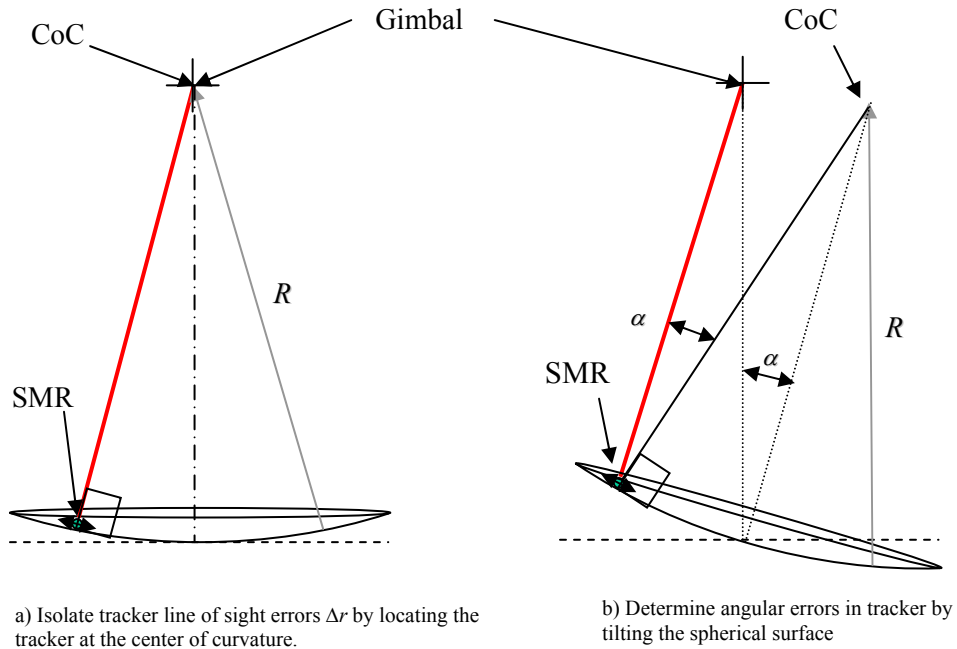


Figure 4. The systematic tracker errors are calibrated over the scan angles using a small concave spherical surface. The radial line of sight errors are determined by making measurements with the sphere aligned to the tracker. The  $x$  and  $y$  angular errors are determined by measuring the sphere with tilt and compensating for the radial errors.

Three measurement steps are used for determining systematic errors in the tracker:

1. Measure the spherical surface with the system aligned so the gimbal axes coincide with the center of curvature of the sphere. Since the measurement line of sight is normal to the surface, errors in angle do not affect this measurement, isolating the radial errors  $\Delta r(\theta_x, \theta_y)$ .
2. Measure the spherical surface with the sphere tilted about the  $y$ -axis and angle  $\alpha_x$ , causing a sensitivity to the gimbal angle  $\theta_x$  which is constant over the surface:  $\frac{dr}{d\theta_x}(\theta_x, \theta_y) = \alpha_x$ . Use this data along with the knowledge of  $\Delta r(\theta_x, \theta_y)$  to calculate  $\Delta\theta_x(\theta_x, \theta_y)$
3. Perform the same measurements as 2) but tilted in the orthogonal direction to determine  $\Delta\theta_y(\theta_x, \theta_y)$

The first attempts at measuring tracker performance are quite promising. A Leica laser tracker model LTD600 was set up at the center of curvature of a 150-mm diameter glass reference sphere as shown in Figure 5. The SMR was moved manually from point to point and a simple fixture was used to keep the SMR from rolling at the measurement points.



Figure 5. Experimental setup with a Leica LTD600 mounted above the test mirror. The mirror is upward facing and the SMR is mounted in a small vacuum fixture designed to hold the SMR firmly against the mirror surface during data collection. Hemostats are used to reposition the SMR between measurements to avoid thermal effects caused by the operator. Each data point is an average of 50 measurements.

The preliminary data from this testing are quite encouraging. The raw data set from a single measurement with the gimbal at the center of curvature shows only  $0.4 \mu\text{m}$  rms variation, which is mostly noise. The low order errors for this single measurement contributes only  $0.047 \mu\text{m}$  rms. (See Figure 6.) The repeatability of these measurements is not quite this good, and the data show much larger noise and systematic effects when the mirror is tilted by  $10^\circ$ . The average from three such measurements is given in Table 1 for the on-axis case, and the results of one measurement each are given for  $x$  tilt and  $y$  tilt. The reported uncertainties were computed using Monte Carlo simulation to establish the relationship between noise in the data and uncertainty in each of the Zernike coefficients that are fit to this data.

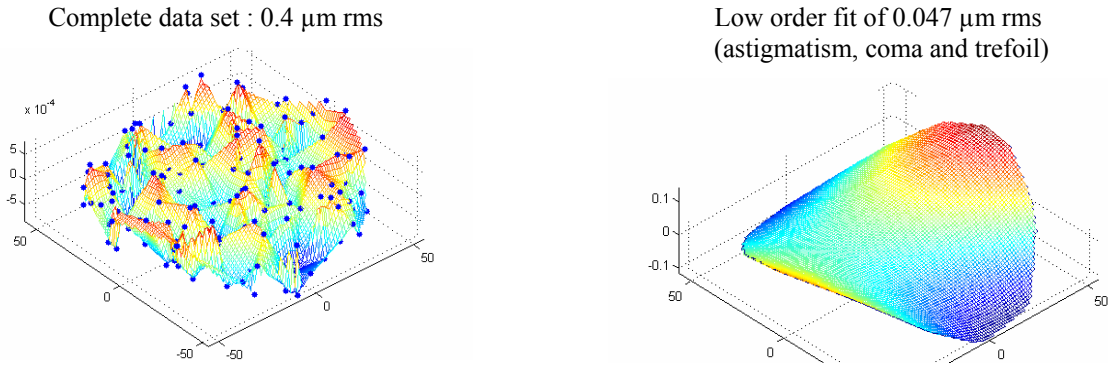


Figure 6. Measurement of tracker errors where the gimbal is aligned to the center of curvature.

Table 1. Errors measured using the laser tracker and a spherical reference surface. All numbers are in  $\mu\text{m rms}$ .

Zernike Aberrations	Configuration 1 (average from 3 data sets)	Configuration 2		Configuration 3	
	$\theta_x = 0^\circ$ $\theta_y = 0^\circ$	$\theta_x = 10^\circ$	$\theta_y = 0^\circ$	$\theta_x = 0^\circ$	$\theta_y = 10^\circ$
Overall	0.46 $\mu\text{m}$	2.1 $\mu\text{m}$		1.5 $\mu\text{m}$	
Astigmatism $0^\circ$	$0.20 \pm 0.12 \mu\text{m}$	$-0.56 \pm 0.2 \mu\text{m}$		$0.16 \pm 0.14 \mu\text{m}$	
Astigmatism $45^\circ$	$0.06 \pm 0.06 \mu\text{m}$	$-0.23 \pm 0.2 \mu\text{m}$		$0.54 \pm 0.15 \mu\text{m}$	
Coma $0^\circ$	$-0.05 \pm 0.11 \mu\text{m}$	$0.68 \pm 0.2 \mu\text{m}$		$0.92 \pm 0.14 \mu\text{m}$	
Coma $90^\circ$	$-0.05 \pm 0.09 \mu\text{m}$	$0.67 \pm 0.2 \mu\text{m}$		$0.17 \pm 0.15 \mu\text{m}$	
Trefoil $0^\circ$	$0.01 \pm 0.08 \mu\text{m}$	$0.20 \pm 0.2 \mu\text{m}$		$-0.08 \pm 0.14 \mu\text{m}$	
Trefoil $30^\circ$	$-0.02 \pm 0.03 \mu\text{m}$	$-0.64 \pm 0.2 \mu\text{m}$		$0.23 \pm 0.16 \mu\text{m}$	
For fit of all terms	0.22 $\mu\text{m}$	1.3 $\mu\text{m}$		1.1 $\mu\text{m}$	

The measurements always tend to show drift with time. This can be corrected by removing the linear time dependence as long as the trajectory of the surface measurements does not have a systematic bias that would cause real surface features to appear as drift in the data. Figure 7 below shows an example of data that was taken over a random grid, allowing the  $2 \mu\text{m}$  drift to be fit and removed.

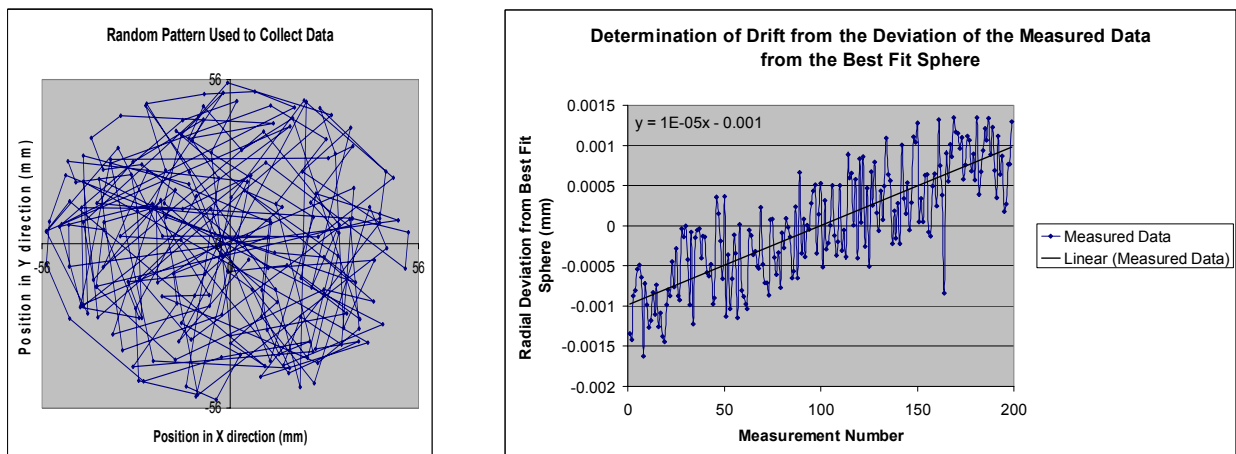


Figure 7. The trajectory of the SMR across the mirror surface, which allows the effect of drift to be fit and removed directly.



The use of the laser tracker for surface measurements builds on the experience from measuring a 1.7-m off axis parabola.<sup>3</sup> The grinding of this surface was guided with the laser tracker exclusively. Once it was polished, the mirror was measured using optical interferometry, which matched the tracker measurement to about 0.5  $\mu\text{m}$  rms. Like the GMT, the tracker was not mounted at the center of curvature, but unlike GMT, there was no attempt to calibrate the tracker or to compensate real time for changes in the line of sight distance or angle. The 1.7-m diameter mirror has 7.7-m radius of curvature and the tracker was mounted about 2 meters above the mirror. The sensitivity to angle for this geometry is 0.44  $\mu\text{m}/\text{arcsec}$ . (This sensitivity was calculated using a more exact relationship for this case since the small angle approximations made above would not be valid for this geometry where the tracker is so close to the mirror.)

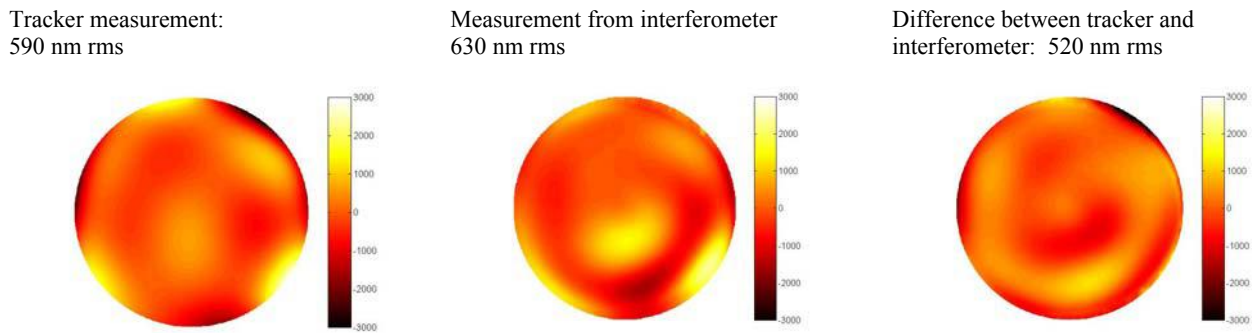


Figure 8. The laser tracker measurements of the 1.7-m off axis parabola agree to 0.5  $\mu\text{m}$  rms with data from the interferometer. The low order terms of power, astigmatism and coma, which are strongly affected by alignment, were removed from this data.

Using the combination of off-line calibration of tracker errors, noise reduction, and real-time measurement of line of sight distance and angle changes, we have set an ambitious goal of measuring each of the low order modes of astigmatism, power, coma and trefoil to  $< 0.2 \mu\text{m}$  rms. This will corroborate the lowest order terms for the optical test to a level that corresponds to the ability to correct these modes in the telescope. Higher order modes can be corroborated using the shear test.

### 3. SLOPE MEASUREMENTS USING SCANNING PENTAPRISM SYSTEM

The analysis of the principal interferometric optical test shows that it can measure the figure and geometry of the GMT segment to the required accuracy in all respects. We are confident that the laser tracker system above will achieve  $\sim 1 \mu\text{m}$  accuracy to guide the coarse figuring and we are hopeful that the continuing development will allow this system to achieve  $\sim 0.25 \mu\text{m}$  accuracy, which would be sufficient for corroborating the low order modes. However we recognize that we cannot rely on such improvement without subjecting the GMT project to significant risk. The scanning pentaprism system provides an independent measurement that can be developed with very little risk. The requirements for GMT testing are actually much less stringent than what we have achieved on similar projects

The pentaprism test, illustrated in Figure 9, measures slope errors in a series of one-dimensional scans across the segment. It does this by projecting a collimated beam parallel to the optical axis of the parent asphere and measuring the position of the focused spot on a detector at the focus of the parent. A beam projector introduces the beam perpendicular to the axis, and the pentaprism deflects it by  $90^\circ$ . This test was successfully performed at the University of Arizona for the 1.8-m  $f/1$  VATT primary<sup>4</sup> and has been subsequently developed to calibrate a 6.5-m optical system.

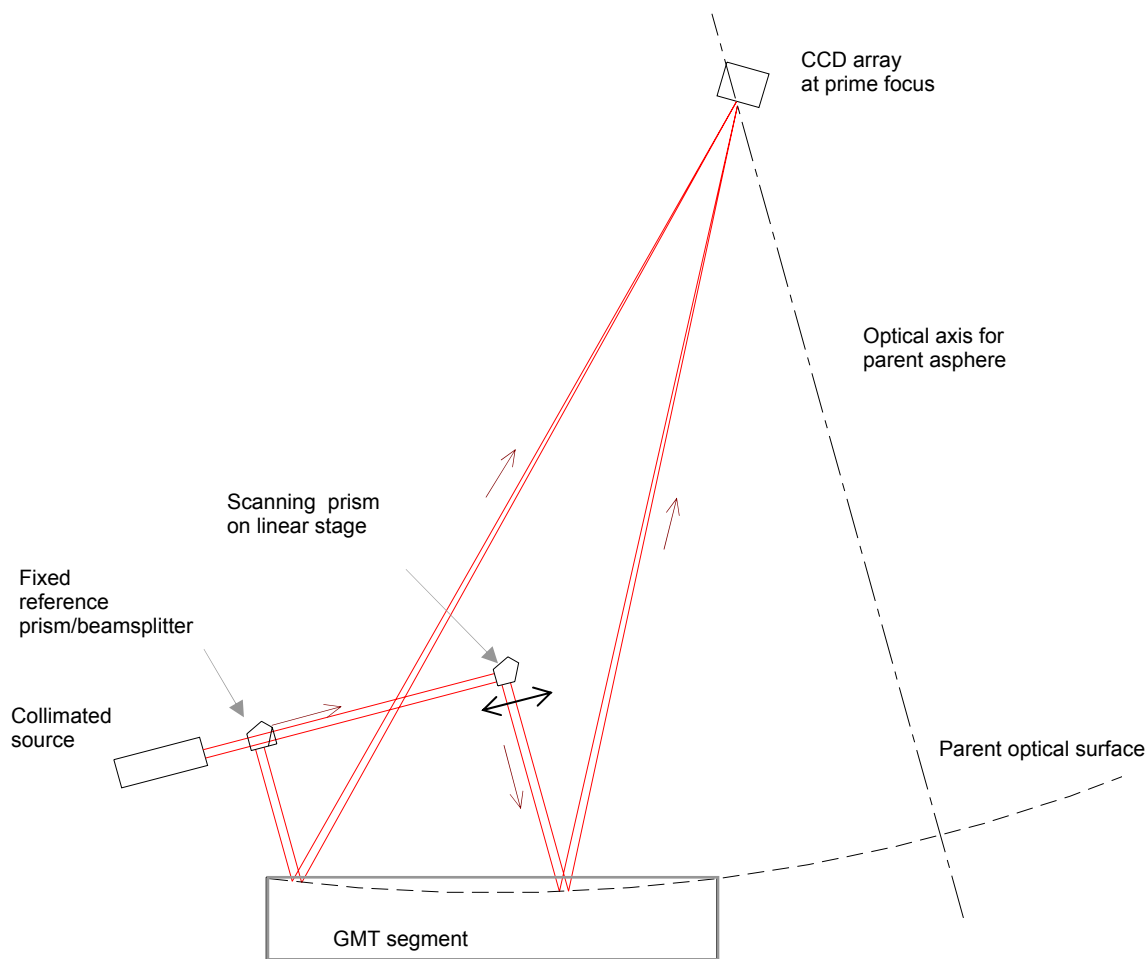


Figure 9. The scanning pentaprism test uses reflection from pentaprism to project a 50 mm beam of light to the primary mirror in the direction parallel to its optical axis. For an ideal paraboloidal mirror perfectly aligned, the light will be imaged to prime focus, the focal point of the mirror. Slope errors in the mirror cause this image to move as the pentaprism is driven across the diameter of the mirror.



The properties of the pentaprism make the surface slope measurement nearly immune to errors in motion of the pentaprism. Figure 10 illustrates these properties. The beam's deflection in the pitch direction is independent of small rotations of the pentaprism, so high accuracy is maintained as the pentaprism scans across the surface. This accuracy holds only for the component of slope parallel to the scan direction, so the slope in the perpendicular direction is ignored. The measurement *is* sensitive to changes in the pitch of the beam projector, so we mount a fixed pentaprism beamsplitter in front of the beam projector and measure the relative positions of the spots formed by the two pentaprisms.

A single scan of the surface will measure slope errors in one direction along one diameter of the segment. We combine scans taken at several angles to determine the global shape errors in the surface. A least-squares fit provides the surface error as a set of Zernike polynomials.

The scanning pentaprism system will measure the low-order aberrations that are most sensitive to alignment errors in the principal optical test. Data from four scans positioned at 45° intervals would allow focus, astigmatism, coma, trefoil and spherical aberration to be determined. Accuracy requirements for these low order errors are based on the same criterion as those for the principal optical test – residual errors in the segment must be correctable by translating and bending the segment – using displacements and correction forces within the allowed limits.

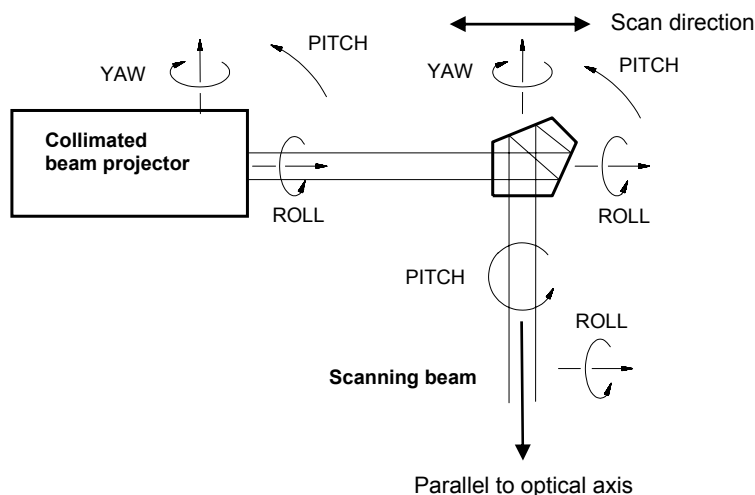


Figure 10. Definition of degrees of freedom for the scanning pentaprism. The measurement is sensitive to errors in pitch of the scanning beam, which is to first order independent of pitch, roll and yaw of the pentaprism.

Because focus, astigmatism and coma are sensitive to the segment's position relative to the optical axis, the pentaprism test includes a laser tracker measurement of the position of the segment relative to the detector at the focus. The test thus measures the geometry of the segment—radius of curvature, off-axis distance, and clocking angle— independently of the principal optical test.

The scanning pentaprism test gives a null result (no spot motion) for a perfect paraboloid. For the slightly ellipsoidal GMT segment, we would measure 10 μrad or 183 μm rms spot motion for a perfect mirror. This desired spot motion is subtracted from the measured motion.

Error analysis for this test shows that a simple system can be built that easily meets GMT requirements. The low order shape errors do not need to be known perfectly because they will be adjusted in the telescope based on wavefront measurements. However, the shape errors must be small enough so they do not use a significant portion of the 50 N actuator force that was budgeted for correction, or that the correction using available bending modes does not leave significant residual shape errors.

Table 2. Top level error budget for the scanning pentaprism test, along with the corresponding budget for a 6.5 m scanning pentaprism system. Values are rms wavefront slope error in nrad.

Source of error	nrad rms
determination of spot position	600
aliasing of mirror figure error	500
optical alignment	500
thermal effects	300
sum in quadrature	975

For a given rms wavefront slope error for each sample, the accuracy with which the aberrations can be measured depends on the number of sample points per scan, the number of scans, and the extent to which errors are correlated among sample points and scans. We have determined the measurement accuracy for each aberration by simulating a complete measurement of four scans, every 45°, and uncorrelated noise of 1  $\mu$ rad rms per point. For nominal sampling of 20 points per scan, we will measure the low order aberrations to the accuracies listed in Table 3. The accuracies listed for astigmatism, coma and trefoil are the net errors, combining both components of each aberration.

Table 3. Predicted error in measurement of low-order aberrations with the scanning pentaprism test. The table also lists the rms correction force and rms surface error after correction.

aberration	rms surface error (nm)	rms correction force (N)	rms residual error (nm surface)
focus	68	2.6	3.7
astigmatism	170	2.2	3.2
coma	60	9.0	8.4
trefoil	120	7.2	5.4
spherical aberration	30	12.6	8.7
sum in quadrature		17.4	14.1

Table 3 also lists the rms force required to correct each aberration with the active support, and the residual error after correction. The correction forces and residual errors are within the budget. This analysis is conservative in that it ignores the partial correction of focus, coma and astigmatism by displacing the segment in the telescope. It does not, however, include the uncertainties in measuring the position of the focal point (where the spot motion is measured) relative to the segment. This position, in 3 dimensions, determines the off-axis distance, clocking angle, and focal length of the segment. It will be measured with a laser tracker after both the scanning rail angle and the position of the detector have been adjusted to minimize alignment aberrations. By measuring positions to an accuracy of 200  $\mu$ m with the laser tracker, we expect to determine the focal length and off-axis distance to 200  $\mu$ m, and clocking angle to 10 arcseconds.

The implementation of the scanning pentaprism test requires some large support hardware. An 8.4 m long carriage must be supported above the segment and rotated to 4 different angles. Alternatively a single frame with 4 rails can be placed over the segment. A CCD detector must be placed 18 m from the segment at the focal point of the parent. This geometry is shown in Figure 11.

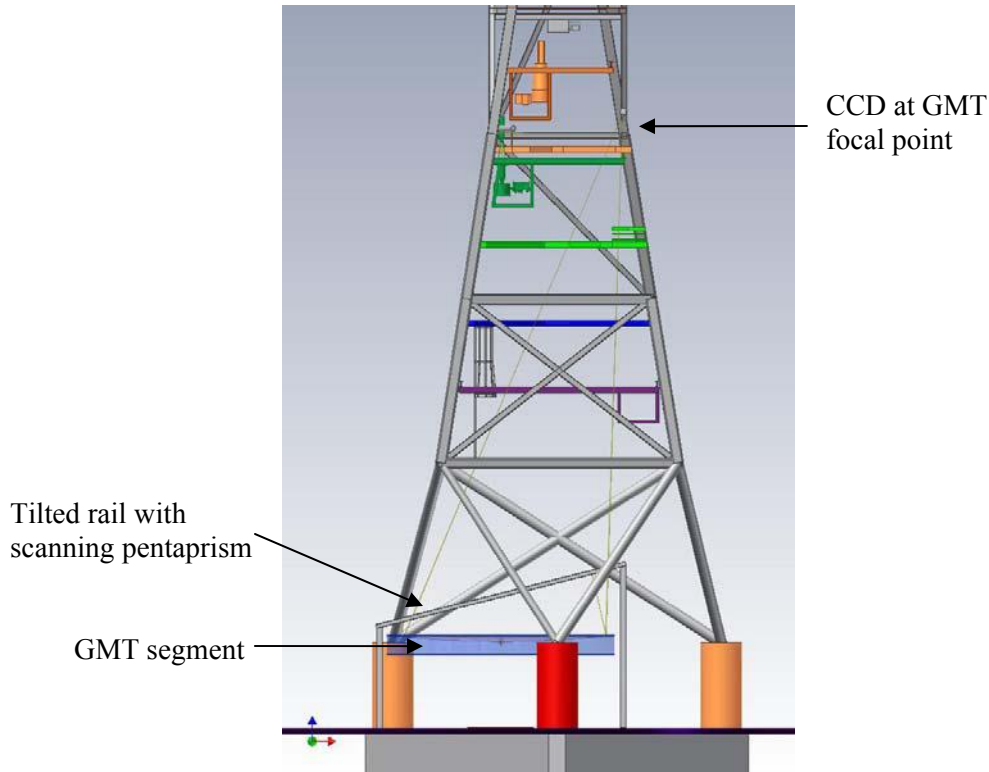


Figure 11. Layout of scanning pentaprism test in the new test tower.

#### 4. MEASUREMENT OF SMALL SCALE ERRORS USING A SHEAR TEST

The symmetry of the segment with respect to rotation about the telescope's optical axis can be exploited to verify the accuracy of the optical test in important respects. The GMT primary mirror is an ellipsoid of revolution, symmetric about the optical axis of the telescope. Each segment possesses this same symmetry about the parent axis. An ideal segment can be rotated about this axis and the apparent shape of the mirror will not change. This geometry is shown in Figure 12. The interferometer views the mirror in fixed coordinates that do not rotate with the segment, so any changes in the apparent shape are due to figure errors that are not symmetric about this axis. This change is independent

of errors in the test system. This technique is a variation of a common method that is used for axisymmetric parts.<sup>5</sup>

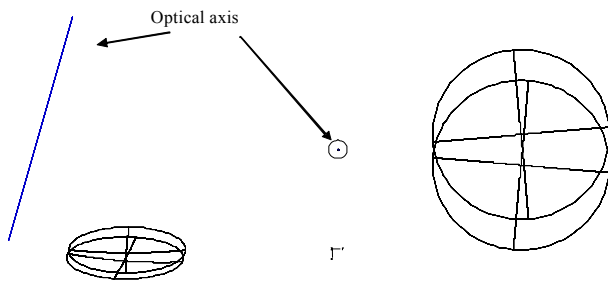


Figure 12. Small scale errors in the test optics can be separated from those in the mirror by rotating the optical surface about its parent axis while the optical test is fixed. Any errors that move with the mirror are known to be in the surface.

While we cannot rotate the segment around the parent axis by large angles, a 60 mrad rotation will provide a sensitive verification of the optical test. A 60 mrad rotation can be made by shifting the segment laterally by 500 mm, clocking it by 60 mrad, and tilting it by 14 mrad ( $\pm 60$  mm across the 8.4-m diameter). The in-plane displacements will be made by moving the segment positioner before parking the segment on it. The positioner is designed with enough vertical travel at each connection to the segment to produce the 14 mrad tilt. The segment's lateral

support will take 1.4% of the weight of the segment, about 250 kg. The lateral support in the polishing cell routinely takes much larger loads from the lap and distributes them to six load spreaders at the back of the segment. The surface distortion resulting from the 250 kg lateral load will be calculated and subtracted from the measured figure change.

Software was developed that optimally estimates the magnitude of features that are both fixed in the test optic and that move with the mirror segment.<sup>6</sup> This software was demonstrated to work to the noise limit of ~3 nm rms for the testing of a 1.6-m flat mirror.

A preliminary analysis of this shear test indicates that it can provide fully redundant information for intermediate scale shape errors, limited only by the few nm random noise in the data. The test has very poor sensitivity for astigmatism, power, coma, and trefoil, but these are the aberrations measured accurately by the pentaprism system.

## 5. CONCLUSION

Accurate testing for the GMT primary mirror is critical for the project. We are now working towards detailed design and hardware fabrication for a set of measurement systems that overlap in their capabilities, assuring that the GMT primary mirror segments meet their performance goals and the production schedule. A summary of the test is given below in Table 4.

Table 4. Alternate optical tests that are planned for the 8.4-m GMT primary mirror segments.

Optical Test	Function	Purpose	Performance
<u>Principal test</u> Interferometry using fold spheres + CGH	Measure entire surface to ~2 cm spatial resolution	Guide polishing, qualify finished surface	Low order: correctable with <25 N rms actuator force Higher order: <30 nm rms surface irregularity
<u>Scanning pentaprism measurements</u>	Measure surface errors corresponding to lowest bending modes	Redundant test for low order shape, including RoC	Lowest order modes: correctable with <20 N rms actuator force
<u>Laser Tracker</u> (plus references)	Measure surface with ~60 cm spatial resolution	Guide coarse figuring Redundant test of shape	~1 μm rms 0.25 μm rms goal
<u>Shear test</u> using principal interferometric test	Shift mirror to allow separation of test errors from mirror features	Redundant test of high order figure errors	< 20 nm rms

## REFERENCES

1. M. Johns, "The Giant Magellan Telescope (GMT)", in *Ground-based and Airborne Telescopes*, ed. L. M. Stepp, Proc. SPIE 6267 (2006).
2. J. H. Burge, L. B. Kot, H. M. Martin, C. Zhao and R. Zehnder, "Design and analysis for interferometric testing of the GMT primary mirror segments", in *Optomechanical Technologies for Astronomy*, ed. E. Atad-Ettingui, J. Antebi and D. Lemke, Proc. SPIE 6273 (2006; these proceedings).
3. H. M. Martin, J. H. Burge, S. D. Miller, B. K. Smith, R. Zehnder and C. Zhao, "Manufacture of a 1.7-m prototype of the GMT primary mirror segments", in *Optomechanical Technologies for Astronomy*, ed. E. Atad-Ettingui, J. Antebi and D. Lemke, Proc. SPIE 6273 (2006; these proceedings).
4. J. H. Burge, *Advanced Techniques for Measuring Primary Mirrors for Astronomical Telescopes*, Ph. D. Dissertation, Optical Sciences, University of Arizona (1993).
5. R. E. Parks, "Removal of test optics errors," in *Advances in Optical Metrology*, N. Balasubramanian and J. C. Wyant, eds., Proc. SPIE 153, 56-63 ~1978.
6. P. Su, J.H. Burge, R. Sprowl, J. Sasian, "Maximum Likelihood Estimation as a General Method of Combining Sub-Aperture Data for Interferometric Testing," in *International Optical Design Conference 2006*, Proc. SPIE 6342 (2006).